AGU PUBLICATIONS

Geophysical Research Letters

RESEARCH LETTER
10.1002/2017GL075685

Key Points:
- *PKP* travel times and their rapid lateral variation for the SSI-Alaska path are related to structure in the lowermost mantle
- A structural boundary with about 3% *P* wave velocity contrast is detected at the lowermost mantle beneath Eastern Alaska
- The heterogeneity layer is not laterally continuous and may terminate beneath Northeastern Alaska

Supporting Information:
- Supporting Information S1

Correspondence to:
X. Long,
longxin@eri.u-tokyo.ac.jp

Citation:
Long, X., Kawakatsu, H., & Takeuchi, N. (2018). A sharp structural boundary in lowermost mantle beneath Alaska detected by core phase differential travel times for the anomalous South Sandwich Islands to Alaska Path. *Geophysical Research Letters*, *45*. https://doi.org/10.1002/2017GL075685

Received 20 SEP 2017
Accepted 27 DEC 2017
Accepted article online 3 JAN 2018

A Sharp Structural Boundary in Lowermost Mantle Beneath Alaska Detected by Core Phase Differential Travel Times for the Anomalous South Sandwich Islands to Alaska Path

Xin Long[1], Hitoshi Kawakatsu[1], and Nozomu Takeuchi[1]

[1]Earthquake Research Institute, The University of Tokyo, Tokyo, Japan

Abstract We report anomalous core phase *PKPbc-PKPdf* differential travel times relative to 1-D spherically symmetric model with a uniformly anisotropic inner core recorded by stations in Alaska for South Sandwich Islands (SSI) earthquakes. The data sample the inner core for the polar paths, as well as the lowermost mantle beneath Alaska. Our major observations are the following: (1) fractional travel time residuals of *PKPbc-PKPdf* increase rapidly within 2°, (2) a clear shift of the residual pattern could be seen for earthquakes with different locations, and (3) the residuals show systematic lateral variation: at the northern part, no rapid increase of residual can be seen. A structural boundary with a *P* wave velocity contrast of about 3% at the lowermost mantle beneath East Alaska is invoked to explain the observation, and the required strength of anisotropy in the quasi-western hemisphere of the inner core might be reduced if those anomalous data are excluded from analysis.

1. Introduction

The lowermost several hundreds kilometers of the mantle is one of the most enigmatic regions in the deep earth. It has many conspicuous seismological features, such as the *D″* discontinuity (Lay & Helmberger, 1983), ultralow-velocity zone (Garnero et al., 1998), and small scatters (Shearer et al., 1998); however, their origins are still not clear.

The presence of such strong variations of the lowermost mantle structure may severely affect the travel times of core phases that are often used to infer the inner core structure. Raypaths of *PKP* phases (*PKPab*, *PKPbc*, and *PKPdf*) are only similar above middle mantle and are quite different in the lowermost mantle, especially for *PKPab* and *PKPdf* (Bréger et al., 2000). If two of them pass through regions with distinctive velocities, their differential travel time would become anomalous with respect to 1-D spherically symmetric model. Sun et al. (2007) has shown such a case, where *PKPdf* and *PKPab* experience fast and slow regions respectively in the lowermost mantle at the source side, resulting in a large variation in their differential travel times. The differential travel times of core phases have been extensively used to explore the seismic structure of the inner core, and it has been found that the inner core has a characteristic of hemispherical dichotomy for velocity, attenuation, and anisotropy (Iritani et al., 2014a, 2014b; Irving & Deuss, 2011; Tanaka & Hamaguchi, 1997; Wen & Niu, 2002). The general anisotropic property of the inner core—the quasi-western hemisphere is more anisotropic than the quasi-eastern part—has been discussed in the seismological literatures; however, there are still some questions about the intensity of anisotropy of the quasi-western hemisphere of the inner core. Data from South Sandwich Islands (SSI) to Alaska paths dominate strong anisotropy in this region and are critical to constrain the strength of anisotropy in the inner core (Deuss, 2014). For those paths, *PKPbc-PKPdf* travel time residuals are anomalously larger than data that sample other regions (Tkalčić et al., 2002), and strong biases from mantle (or the outer core) heterogeneities are suggested by several previous studies (Bréger et al., 2000; Romanowicz et al., 2003; Romanowicz & Wenk, 2017); if SSI data are removed, the global average of inner core anisotropy strength becomes much smaller (Leykam et al., 2010), and a constant anisotropy model can fit both normal mode and travel time data quite well (Ishii, Dziewonski, et al., 2002, Ishii, Tromp, et al., 2002). The *PKP* residuals for data from SSI earthquakes also have a strong lateral variation (from 1 to 4 s) which has been noted by Tkalčić (2010), and a contribution from the lowermost mantle at source side has been considered as a possible cause for such a variation. For those reasons, the raypaths from SSI to Alaska are often considered as disputed (Romanowicz et al., 2003; Romanowicz & Wenk, 2017), and no consensus

has been resolved among researchers, probably due to sparse station coverage until recently (both at SSI and Alaskan sides). As a result, a robust bound on the strength of anisotropy in the quasi-western hemisphere of the inner core cannot be obtained. Recent global *P* wave (Young et al., 2013) and regional *S* wave tomography (Suzuki et al., 2016) researches targeting lowermost mantle show large velocity variation (about 3%) just beneath Alaska. If the horizontal scale of the anomaly is as small as several hundred kilometers, that might be smeared in global tomography models, and velocity variation could be even larger. Raypaths of *PKP* waves from SSI earthquakes also pass this region at lowermost mantle, so the large variation of *PKPbc-PKPdf* residual may be due to the heterogeneity in the lowermost mantle at the receiver side.

In this research, we use core phase travel time data from the SSI earthquakes to investigate the lowermost mantle structure beneath Alaska. The current dense seismic stations in Alaska enable us to conduct a detailed investigation for this region, and short period *PKP* waves has good lateral resolvability for small-scale heterogeneities. By analyzing the variation of *PKPbc-PKPdf* residual patterns, we demonstrate that the existence of a structural boundary beneath eastern Alaska can explain the observed steep increase of *PKPbc-PKPdf* travel time residuals and may reduce the required strength of anisotropy in the quasi-western hemisphere of the inner core.

2. Data and Observation

Data used in this research are from the Alaska regional network and current USArray, and the number of available stations is nearly 200 in total (Figure 1a). Such dense station coverage provides us a good opportunity to investigate the lowermost structure beneath Alaska. Distances from these stations to SSI earthquakes are mainly within a range of [145°, 154°], and 612 pairs of *PKPdf* and *PKPbc* phases for nine events in the SSI region and one in Southern Mid-Atlantic Ridge (Table S1 in the supporting information) are collected. Seven of those SSI earthquakes are located close, and distances among them are less than 1°; their depths are also relatively greater (~100 km). We refer to them as "main SSI event group" hereafter. All the waveforms are handpicked and instrument responses deconvolved, and a two-pole Butterworth band-pass filter of 0.5–2 Hz is applied. An example of the data is shown in Figure 1b, and it could be noted that *PKPdf* suddenly become faster and weaker around 148°.

The collected *PKPdf* all travel along the polar path, and for the main SSI event group, the angle ξ between the raypaths and rotation axis of the Earth are mainly within [25°, 28°]. The *PKPbc-PKPdf* differential travel time is measured using times of the peaks of *PKPbc* and *PKPdf* waveforms that have the same polarity on the vertical component. Due to attenuation of *PKPdf* in the inner core, the peak-to-peak differential travel time is slightly different from the true differential arrival time between *PKPbc* and *PKPdf*, so we also measured the differential travel time by a simulate annealing waveform inversion method (Iritani et al., 2014a). The measurements by these two methods only have a small systematical difference about 0.1 s, so we consider the measured peak-to-peak *PKPbc-PKPdf* differential travel times are reliable. A differential travel time residual of *PKPbc-PKPdf* relative to 1-D ak135 model (Kennett et al., 1995) is defined as

$$\delta t = \left(t_{\mathrm{bc}}^{\mathrm{obs}} - t_{\mathrm{df}}^{\mathrm{obs}}\right) - \left(t_{\mathrm{bc}}^{\mathrm{ak135}} - t_{\mathrm{df}}^{\mathrm{ak135}}\right), \tag{1}$$

where *t* denotes the travel time of observed or predicted by ak135 (superscript) of *PKPbc* or *PKPdf* (subscript) phase.

The contributions to the residual are mainly from the inner core and/or the lowermost mantle. Such effects may be characterized by the fractional residual, a ratio of the differential travel time residual to the total travel time in each region. To simplify the analysis, we assume that anisotropy of the inner core is uniform and axisymmetric, then the consequent fractional residual for a given ray angle ξ could be modeled by

$$\frac{\delta t_{\mathrm{IC}}(\xi)}{t_{\mathrm{IC}}} = a + b\ \cos^2\xi + c\ \cos^4\xi \tag{2}$$

as commonly employed in previous related researches (Creager, 1992; Irving & Deuss, 2011, 2015; Shearer & Toy, 1991; Sun & Song, 2008); here $\delta t_{\mathrm{IC}}(\xi)$ is the differential travel time residual due to the inner core structure, t_{IC} is the total travel time of the DF path in the inner core, and *a*, *b*, and *c* are constants. If only the inner core contributes to the residual and ξ does not have much variation, then the fractional residual should not depend on distance much and be approximately constant.

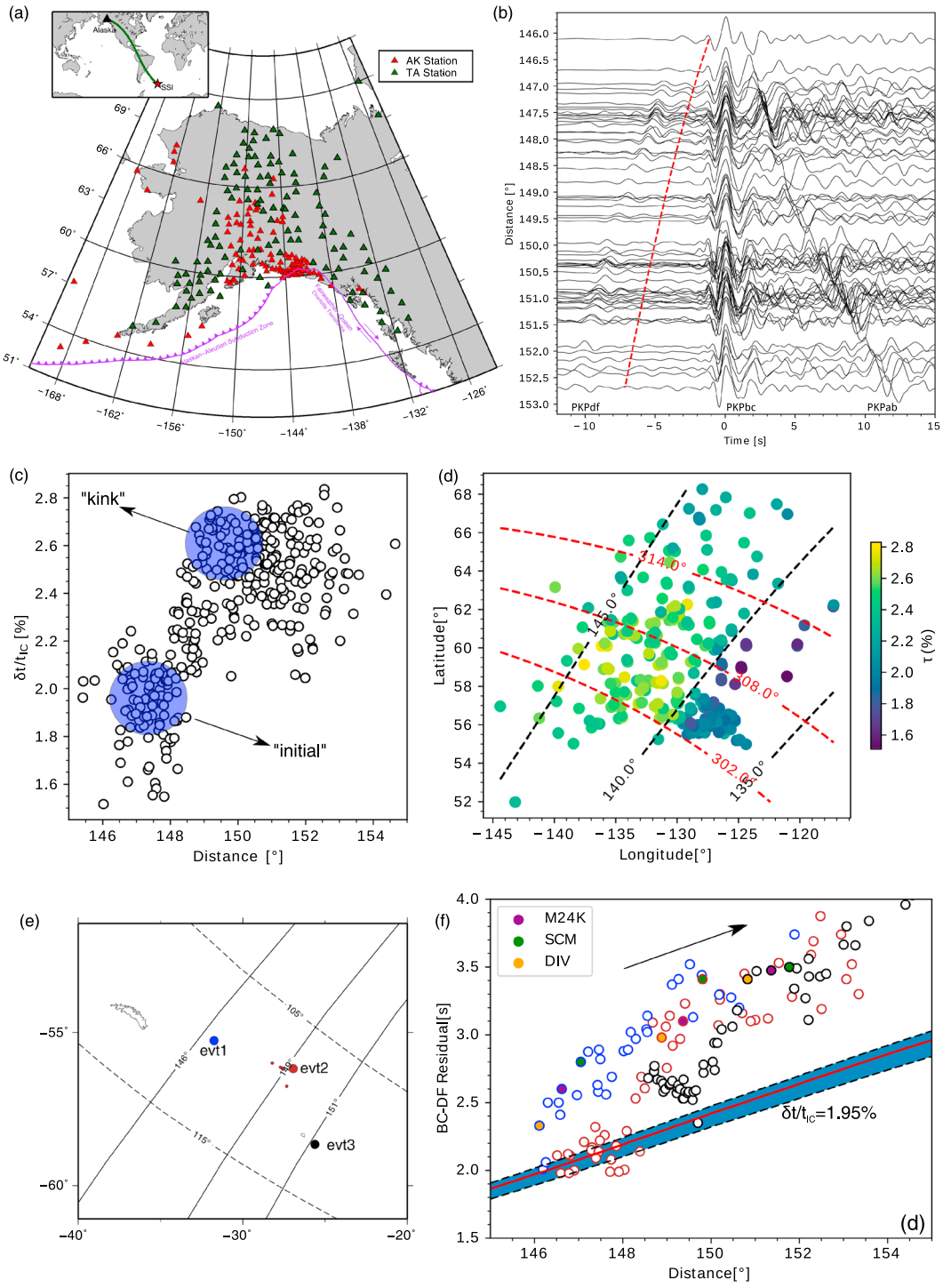

Figure 1. Data used and typical observations in this research. (a) Station distribution of the Alaska regional network and current USArray. The purple curve shows the current Alaska-Aleutian trench and Fairweather-Queen Charlotte transform fault (Bird, 2003). Inset is a representative great-circle path from SSI to Alaska. (b) Waveforms recorded by AK stations for event 1 February 2014. The records are aligned by peak time of *PKPbc*, and the red dashed line is the *PKPdf* arrival time predicted by ak135. (c) Observed *PKPbc-PKPdf* fractional residuals for seven earthquakes in the main SSI event group. Distance correction to a surface source has been made for those events. For most of the data, ξ is mainly within [25°, 28°]. Initial and kink parts of the residual pattern are marked by transparent blue circles. (d) Fractional residuals in Figure 1c plotted at *PKPdf* piercing points at CMB. Black and red dashed lines are distance and azimuth contours for evt2. (e) Locations of evt1, evt2, and evt3. Black line and dashed line are contours of distance and azimuth from a fixed station KLU to earthquakes. Small brown dots are locations of the other six main SSI event group events. (f) *PKPbc-PKPdf* residuals for evt1, evt2, and evt3 in Figure 1e where azimuth ranges of [307°, 312°], [303°, 308°], and [299°, 304°] are respectively chosen. Shaded area is residual predicted by the QWH model of Irving and Deuss (2011), and the red line stands for fractional residual of 1.95%. The filled circles are data points picked in the kink part of the residual pattern for the three events, and each color represents for the same station.

Figure 1 summarizes the observation of the differential travel time residuals of *PKPbc-PKPdf* for the SSI events. For the main SSI event group, the fractional residual $\delta t/t_{IC}$ increases rapidly from 1.6% to 2.8% within distance range of [147.5°, 149.5°] (Figure 1c), and a lateral variation from south to north, when plotted at the receiver side *PKPdf* piercing points at the core-mantle boundary (CMB), can be also observed (Figure 1d). A similar variation of the *PKP* absolute travel times has been observed by Romanowicz et al. (2003). According to the quasi-western hemisphere (QWH) inner core anisotropy model of Irving and Deuss (2011) and equation (2), the variation of fraction residual for ξ within [25°, 28°] should be less than 0.4% even when the inner core anisotropy is as strong as 4.8%. An inner core with uniform anisotropy alone, therefore, cannot produce such a large and steep increase of *PKPbc-PKPdf* fractional residuals, and the observation requires other causes, such as an abrupt change in the upper inner core structure or some contribution from the lowermost mantle. It could be also noted that the QWH model proposed by Irving and Deuss (2011) and the model of Song and Helmberger (1993) with relatively weak anisotropy of 3% well explain the fractional residual when the distance is smaller than 148° (Figure S11).

Further interesting observation is a shifting of the *PKPbc-PKPdf* residual pattern. When we compare the residual pattern of the main SSI event group with those of the other two earthquakes in Table S1, we find that the residual patterns share a similar steep increase within 2° that happens at different distances. Figure 1e shows the location of events 21 August 2016 (evt1), 2 August 2016 (evt3), and 28 May 2016 (evt2) in the main SSI event group. Distances to a fixed station from evt1 and evt3 differ by about 3° and 2° with that from evt2, and they are comparable with the intervals between the residual patterns. Figure 1f shows the *PKPbc-PKPdf* residual for each of them with the prediction of the model of Irving and Deuss (2011) for evt2. A clear shifting of *PKPbc-PKPdf* residual pattern roughly along the slope of the residual predicted by the anisotropy model could be seen. For those three earthquakes, *PKPdf* that correspond to the "kink" and "initial" parts of the residual pattern (Figures 1c and 1f) sample almost the same regions at the lowermost mantle and even are recorded by the same stations. This is not surprising, because for a given receiver, *PKPdf* receiver-side piercing points at CMB are close for sources with different locations. Further, the relative location of those three picked stations in the kink part of each residual pattern shows a systematic slight shift reflecting the slight difference of actual raypaths relative to the anomaly and demonstrates the robustness of the residual pattern observation. We pick stations roughly corresponding to the initial and kink parts of the residual pattern and find that they are located approximately parallel to the distance contour line of 149° for evt2 (Figure S2), which may suggest a related structure that causes the observed anomalous *PKPbc-PKPdf* residuals also has a linear feature parallel to the distance contour. Fresnel zones of 1 Hz *PKPdf* at CMB and ICB are about 200 and 150 km, respectively. In the inner core, difference in depth of turning points for *PKPdf* at 147.5° and 149.5° is only 35 km, and their piercing points at inner core boundary (ICB) are separated by only about 50 km. If the observed anomaly is due to a rapid structural variation in the inner core, the anomaly must be restricted within a small ray tube, and larger velocity perturbation is required for heterogeneity in the inner core than in the lowermost mantle. Creager (1997) showed a lateral gradient in isotropic velocity in the inner core along east-west direction beneath Columbia could explain the temporal variation of *PKPbc-PKPdf* residuals for station COL; however, the gradient along distance in their model is not strong enough to explain the steep increase of the *PKPbc-PKPdf* residual within 2°. So it seems unlikely that some structure in the upper inner core leads to such shifting, and here we consider a velocity boundary at the lowermost mantle to explain the steep increase of *PKPbc-PKPdf* residuals.

3. Modeling for Travel Time

The most important characteristic of the observed *PKPbc-PKPdf* residual anomaly is its rapid increase within a short distance range, even though some lateral variations also exist. For evt2 of the main SSI event group, the most robust increase exists within the azimuth range of [303°, 308°]. To explain the observed increase, we first introduce a simple high-velocity anomaly in the lowermost mantle at receiver side, whose boundary is parallel or subparallel to the distance contours (Figure 1d). We prefer a receiver side heterogeneity because it is compatible with the observed shifting of the residual pattern for the three events (At the source side, *PKPdf* piercing points at CMB are separated by several degrees for those events. *PKPbc* and *PKPdf* piercing points also intertwine, which would make residual patterns inconsistent for the three earthquakes if the heterogeneity is at source side). At smaller distances, *PKPdf* begins to cross the boundary between the anomaly and the background mantle, while BC still stays in the relatively slow region (Figure 2a). This results in an

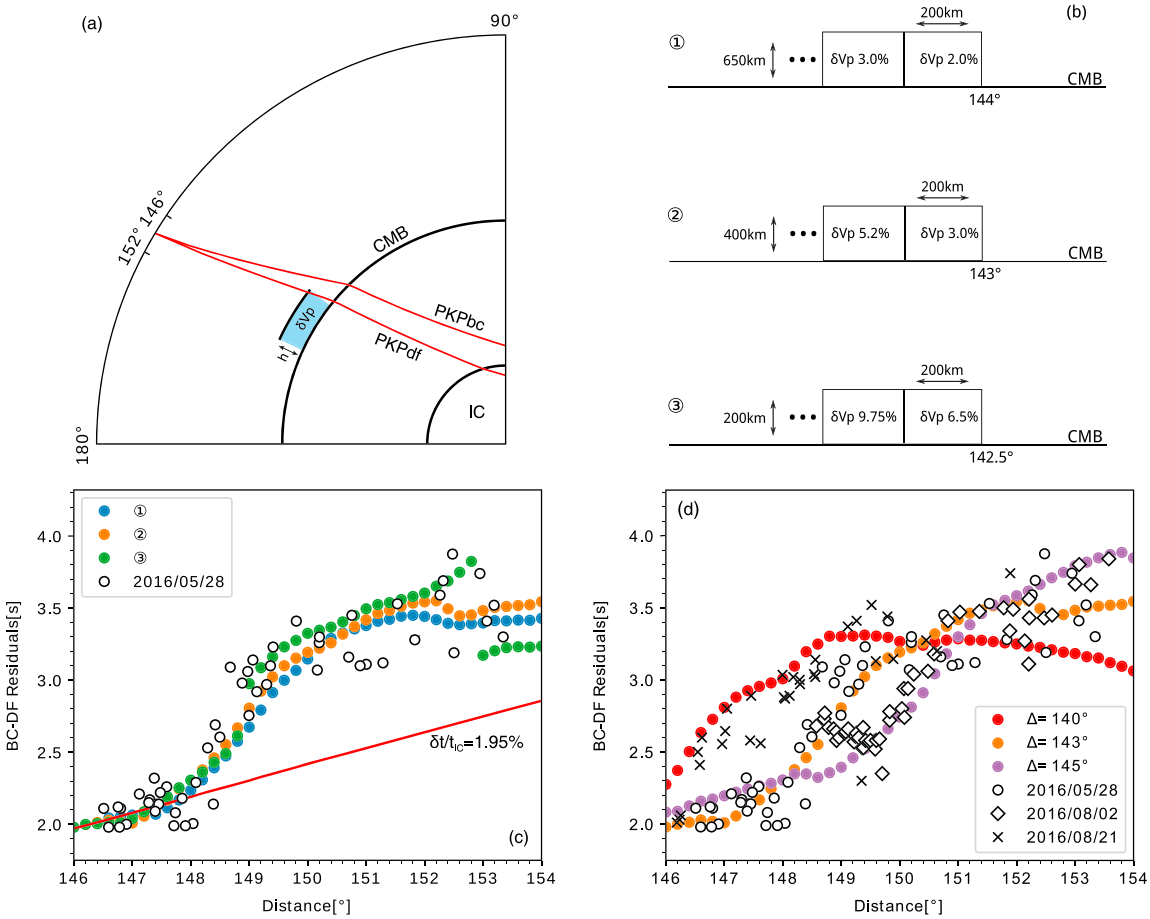

Figure 2. Modeling for *PKPbc-PKPdf* travel time residuals. (a) Basic geometry of the modeling. The light blue region corresponds to the high-velocity heterogeneity with thickness of *h* and a velocity perturbation. *PKPdf* crosses the boundary before *PKPbc* that results in anomalous *PKPbc-PKPdf* residuals. (b) Models of heterogeneity with different thickness and locations (distances). (c) Comparison between observed and synthetic *PKPbc-PKPdf* travel time residuals for the three models in Figure 2b. (d) *PKPbc-PKPdf* residuals modeled for different source locations. Their distances to the heterogeneity are 140°, 143°, and 145°, which correspond to evt1, evt2, and evt3, respectively. Model 2 in Figure 2b is used, and data in Figure 2d are also plotted for comparison.

increase of *PKPbc-PKPdf* residual with distance. If the boundary is sharp enough, the increase becomes steep. The heterogeneity is characterized by its thickness *h*, *P* velocity perturbation δV_p, and the distance of the boundary. We conduct 2.5-D spherical modeling by using AxiSEM code (Nissen-Meyer et al., 2014) that simulates 3-D wavefield for an axisymmetric spherical model using a parallel spectral element method. We first compute for a background model without the heterogeneity, then for a model with it. The background model is AK135 with an inner core that has uniform axisymmetric anisotropy (the global model of Irving & Deuss, 2011). Including an anisotropic inner core at this stage is to avoid the effect due to the change of raypaths, and we make an approximation by assuming that the symmetry axis of the inner core anisotropy and the raypaths are in the same meridian plane (see modeling details in the supporting information). After that, the relative differential travel time of *PKPbc-PKPdf* and *PKPdf* due to the pure effect of the heterogeneity can be obtained. The differential travel time is measured by the same way as we do for the real data, which should reduce the aforementioned bias of the measurements.

In order to fully characterize the *PKPbc-PKPdf* residual, we further incorporate the effect of the lateral (hemispherical) heterogeneity of inner core anisotropy by using equation (2). We use the QWH model from Irving and Deuss (2011), where *a*, *b*, and *c* in equation (2) are −0.0071, −0.0196, and 0.0676, respectively. This model well predicts the *PKPbc-PKPdf* residuals before the steep residual increase (the initial part), which we assume to result from the pure effect of the inner core anisotropy (in fact, the inner core model can be chosen arbitrarily, if it can explain the initial part of the data, because we only try to explain the variation of the residual). Then, the total residual is obtained by combining the effects of the heterogeneity at lowermost mantle and

the inner core anisotropy. After some tests, we found that a simple heterogeneity with a uniform velocity perturbation and constant thickness whose boundary located at a distance of 143° can explain the steep increase of the *PKPbc-PKPdf* residual; however, when PKPbc begins to cross the boundary, the residual would decrease rapidly at distance larger than 151°, which is not observed. This suggests that the heterogeneity may have lateral variation, either in velocity or in thickness. To reconcile the modeling result with observation, we divide the heterogeneity into two parts and make the farther part faster, which compensates the effect of *PKPbc* (Figure 2b). In addition to *PKPdf*, we can see that *PKPab* changes its slowness at distance around 151° (delay of *PKPab* relative to *PKPbc* increases), and this also may be due to the fact that *PKPbc* enters the anomaly (Figures 1b and S9).

The results for different combination of heterogeneity parameters (Figure 2b) are shown in Figure 2c, and a structural boundary with a 3% *P* wave velocity perturbation and 400 km height at 143° can well reproduce the observed residual pattern. There are trade-offs between these parameters, and the size and location of the heterogeneity could not be determined accurately. A thicker layer would require the boundary to be located at larger distance with a smaller velocity contrast, which means the boundary needs to move westward in real geographic coordination; for a thinner layer, an opposite behavior of the boundary would be expected. The heterogeneity layer should not be too thin (e.g., less than 200 km); otherwise, large velocity perturbation is required to produce residual variation larger than 1 s. However, a large velocity perturbation would result in a severe distortion of *PKP* waveforms when they interact with the boundary, especially *PKPbc*. Then it is impossible to measure peak arrival times from synthetic seismograms (Figure 2c). Nevertheless, it is still a little difficult to constrain the thickness of the heterogeneity layer, and for example, the residual patterns for a layer with thickness of 400 km and 650 km do not show significant difference (Figure 2c). However, if the observed and modeled *PKPdf*/*PKPbc* amplitude ratios are compared, it could be noted that model with a 400 km thick heterogeneity predicts the location of the minimum of the amplitude ratio better (The minimum for Model 2 is at about 149.4°; however, that for Model 3 is at 150°; see Figure S3). The reduction of the ratio is probably due to defocusing of *PKPdf* when it interacts with the boundary.

The shifting of the residual pattern in Figure 1f can also be well reproduced by the model, if we change the location of source and fix the location of the heterogeneity. Figure 2d shows the modeled *PKPbc-PKPdf* residual patterns for different source locations. Model 2 in Figure 2b is used. The three distances correspond to evt1 (140°), evt2 (143°), and evt3 (145°), respectively. For those modeling, we choose fractional residuals of 2.0%, 1.95%, and 2.06% for those sources (Those values correspond to averages of ξ among the stations for the three events within azimuth ranges of [307°, 312°], [303°, 308°], and [299°, 304°], respectively.).

4. Discussion and Conclusion

We have invoked a structural boundary at the lowermost mantle to explain the observed steep increase and shifting of *PKPbc-PKPdf* differential travel time residuals, and by combining the effects of a uniformly anisotropic inner core and the boundary, the observation could be basically reproduced (Figures 2c, 2d, S4, and S10). However, the lateral variation of the residual is also clear. For all the earthquakes used in this research, the rapid increase of the *PKPbc-PKPdf* residual could not be seen at large azimuth that corresponds to northern part beneath Alaska, and the residuals there are close to the prediction of the uniform anisotropy model used in the modeling. Figure 3 shows the *PKPbc-PKPdf* residual patterns within three different azimuth ranges for evt1, evt2, and evt3. The azimuth-dependent variation seems consistent for these earthquakes. The sampling region can be roughly divided into three azimuth corridors. In the reference framework of evt2, they are Az $<$309°, Az$\in$[310°, 315°], and Az $>$315°, and columns in Figure 3 correspond to these corridors respectively from left to right. For each column, *PKPdf* piercing points are roughly within the same azimuth corridor (Figure S5).

Within the first and second corridor, the steep increase of the residual could be seen, and it is not obvious within the third one. Further, the residuals for the third corridor are relatively smaller compared to those for the other two. The sudden disappearance of the steep increase trend of the residual in the third corridor may indicate that *PKPbc* and *PKPdf* experience no differences and suggest the termination of the heterogeneity; that is, only inner core anisotropy dominantly affects the *PKPbc-PKPdf* residual. Yao et al. (2015) described a similar observation for the *D″* discontinuity beneath the North Atlantic. They found no *Scd* refraction at eastern side of their sampling region and inferred that this might be due to the refracted waves propagate beyond the eastern edge of the Farallon plate. It also could be noted that there is a discrepancy

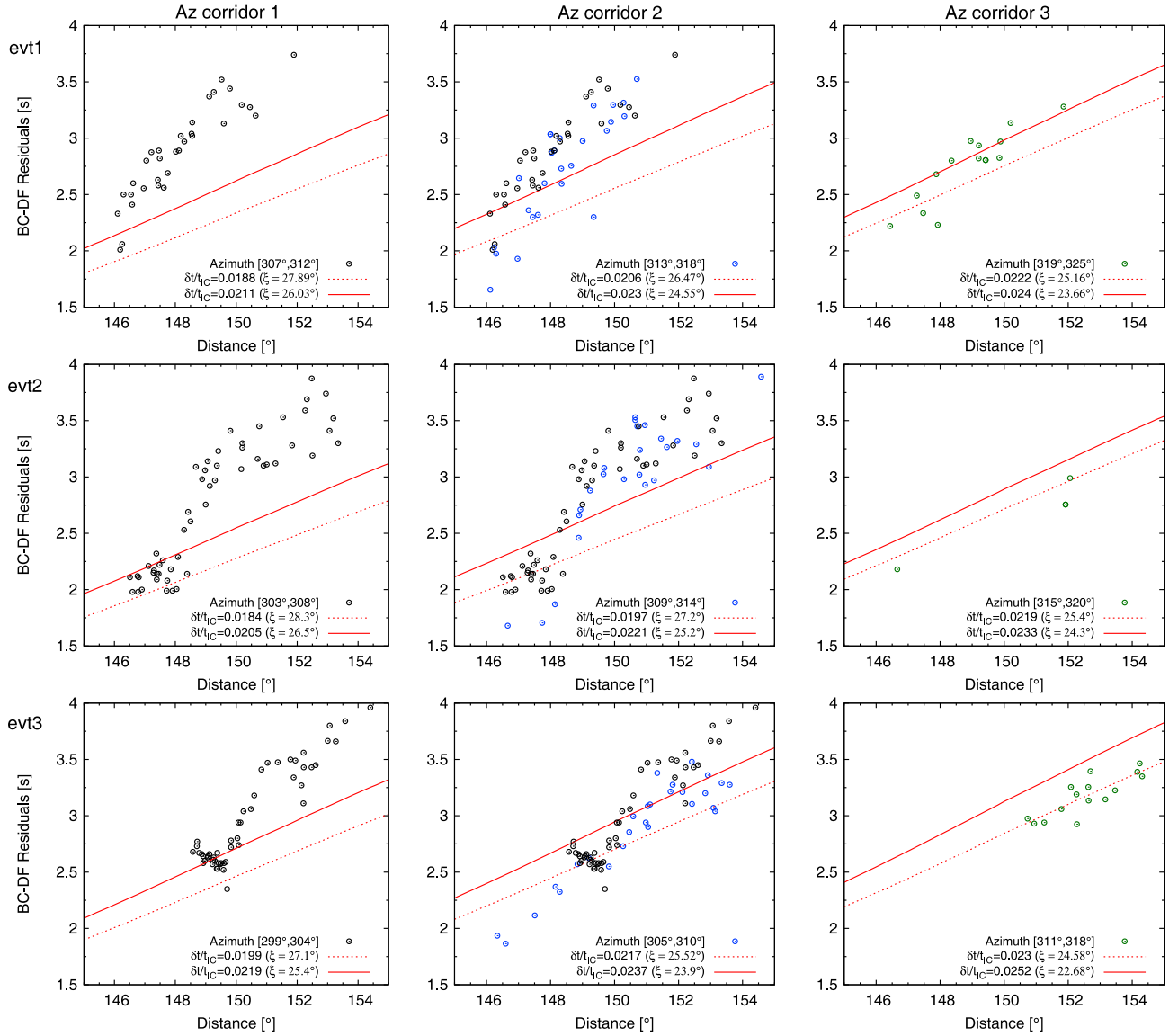

Figure 3. *PKPbc-PKPdf* residuals for evt1, evt2, and evt3 are divided into three corridors according to location of *PKPdf* piercing points (Figure S5). Each column corresponds to one corridor, and each row corresponds to data for one event. Within each azimuth range (i.e., corridor), upper and lower bounds (corresponding to maximum and minimum of ξ within the corridor) of pure inner core effects predicted by the QWH model of Irving and Deuss (2011) are plotted as red line and dashed line, respectively. For comparison, the residuals in the left column are superimposed on the middle column for each event (black circles).

between the residual patterns corresponding to the first and second azimuth corridors. Residuals for the second corridor are systematically 0.2–0.4 s smaller than the prediction of the uniform anisotropic inner-core model, but their residual patterns are similar (Figure 3, middle column). This discrepancy is especially clear for the main SSI event group (Figures 3, middle row, and S6) and may be due to effect of a localized fast heterogeneity on the *PKPbc* paths. If only *PKPbc* is affected by this heterogeneity, then the residual would become smaller systematically. For comparison, we measure the *PKPbc-PKPdf* residual for the Southern Mid-Atlantic Ridge earthquake; if the data for this event are confined within the second azimuth corridor, we can also see a similar residual pattern that has a steep increase part (Figure S7a). This further confirms our major observation, because the *PKPbc* and *PKPdf* piercing points for this event within the second corridor are similar to those for evt2 (Figure S7b). However, the residual is much smaller than the prediction of the anisotropic inner-core model (about 1 s difference at 148°). This could be partly explained by the localized heterogeneity, but a regional structural variation of the inner core may also contribute to some extent (Irving & Deuss, 2015).

The observations suggest a possible lateral variation of the heterogeneity along east-west direction, because a constant layer cannot explain the *PKPbc-PKPdf* residual at larger distance (Figure S8a) as we mentioned earlier. In previous section, we make the heterogeneity 2.2% faster at the farther part of the heterogeneity to compensate the effect of *PKPbc*, and this can also be done by making the farther part thicker. When the velocity perturbation of the heterogeneity is fixed to 3%, a similar residual pattern could be obtained if we increase its thickness from 400 to 700 km at 300 km away from the boundary (Figure S8c). So the lateral variation of the heterogeneity cannot be well constrained. Another question is the sharpness of the boundary. In fact, the velocity gradient is not implemented in current version of AxiSEM; however, we can still make the velocity to increase gradually by dividing the heterogeneity into smaller blocks. We observe that *PKPdf* is not sensitive to the sharpness of the boundary. If the transitional thickness is smaller than 50 km, *PKPdf* residuals seem to be undistinguishable, even though the residuals increase more gradually when the boundary becomes less sharp (Figure S8b). However, a too gradual boundary (e.g., $>$100 km) may be not acceptable, because even the *PKPbc-PKPdf* residuals for the most "sharpest" model is still not steep enough as the observation.

As we have demonstrated, a heterogeneity with 3% *P* wave velocity perturbation and a thickness of 400 km at the lowermost mantle about 143° away from the main SSI event group can basically explain the observed steep increase *PKPbc-PKPdf* travel time residuals, and the residual may also be affected by other small heterogeneities. Some researchers suggest a discontinuity exists in the uppermost inner core, which is due to the transition from weak to strong anisotropy (Song & Helmberger, 1998; Song & Xu, 2002). Such a structure may also cause an increase of the *PKPbc-PKPdf* residuals as a velocity increase about 3.5% at 190 km beneath the ICB would cause about 0.4 s decrease of *PKPdf* travel time from 147° to 149° (Figure S12). However, it could not explain the observed shifting of the residual pattern, and it is also hard to reconcile the observed lateral variation of the residual. In order to reduce the *PKP* travel time up to 1 s as observed, the velocity jump of the discontinuity may need to be over 10%. Such strong anisotropy beneath an isotropy layer about 200 km is not compatible with normal mode observation (Ishii, Dziewonski, et al., 2002). We also do not observe systematical triplication signals caused by an inner core discontinuity, so we conclude that the inner core does not have significant contribution to variation of the residuals. However, small effect of radial structure variation in the uppermost inner core is still possible, and it could increase of the steepness of the differential residual pattern between [147°, 149°].

The inferred thickness of the heterogeneity layer is also close to the height of *D*″ over CMB in the model of Sun et al. (2016). For this region, they observed relatively weaker *Scd* and no obvious *Pcd*, which may suggest the upper boundary of *D*″ layer is gradual. Garnero and Lay (1997) also observed strong anisotropy beneath this region. However, the origin of such heterogeneity is still not clear. It may be related to a subducted ancient slab that have stopped at the CMB as suggest by many studies (Sun et al., 2016; Suzuki et al., 2016; Yao et al., 2015). Recently, there are increasing lines of tomographic evidence for slabs at the CMB (Simmons et al., 2015), so we also consider this as a possibility. However, because of the limitation of the current data set, what we can assure is that a high-velocity anomaly exists beneath Alaska and it significantly affects the *PKPbc-PKPdf* travel time residual. Even though we do not constrain anisotropy of the inner core in the present study, our result might infer that its strength could be reduced for the quasi-western hemisphere if those anomalous SSI-Alaska path core phase data are excluded from analysis.

Acknowledgments

This research is partly supported by JSPS KAKENHI 15H05832. Figures in this paper are produced by GMT (Wessel & Smith, 1991) and Matplotlib (Hunter, 2007). TauP Toolkit (Crotwell et al., 1999) is used to calculate travel times. We thank IRIS for providing the waveform data from network AK (https://doi.org/10.7914/SN/AK) and TA (https://doi.org/10.7914/SN/TA) used in this research. We also thank two anonymous reviewers whose comments helped to significantly improve the manuscript.

References

Bird, P. (2003). An updated digital model of plate boundaries. *Geochemistry, Geophysics, Geosystems*, *4*(3), 1027. https://doi.org/10.1029/2001GC000252

Bréger, L., Tkalčić, H., & Romanowicz, B. (2000). The effect of D″ on PKP(AB−DF) travel time residuals and possible implications for inner core structure. *Earth and Planetary Science Letters*, *175*(1-2), 133–143. https://doi.org/10.1016/S0012-821X(99)00286-1

Creager, K. C. (1992). Anisotropy of the inner core from differential travel times of the phases PKP and PKIKP. *Nature*, *356*(6367), 309–314. https://doi.org/10.1038/356309a0

Creager, K. C. (1997). Inner core rotation rate from small-scale heterogeneity and time-varying travel times. *Science*, *278*(5341), 1284–1288. https://doi.org/10.1126/science.278.5341.1284

Crotwell, H. P., Owens, T. J., & Ritsema, J. (1999). The TauP toolkit: Flexible seismic travel-time and ray-path utilities. *Seismological Research Letters*, *70*(2), 154–160. https://doi.org/10.1785/gssrl.70.2.154

Deuss, A. (2014). Heterogeneity and anisotropy of Earth's inner core. *Annual Review of Earth and Planetary Sciences*, *42*(1), 103–126. https://doi.org/10.1146/annurev-earth-060313-054658

Garnero, E. J., & Lay, T. (1997). Lateral variations in lowermost mantle shear wave anisotropy beneath the north Pacific and Alaska. *Journal of Geophysical Research*, *102*, 8121–8135. https://doi.org/10.1029/96JB03830

Garnero, E. J., Revenaugh, J., Williams, Q., Lay, T., & Kellogg, L. H. (1998). Ultralow velocity zone at the core-mantle boundary. In *The core-mantle boundary region* (pp. 319–334). Washington, DC: American Geophysical Union. https://doi.org/10.1029/GD028p0319

Hunter, J. D. (2007). Matplotlib: A 2D graphics environment. *Computing in Science & Engineering*, *9*(3), 90–95. https://doi.org/10.1109/MCSE.2007.55

Iritani, R., Takeuchi, N., & Kawakatsu, H. (2014a). Intricate heterogeneous structures of the top 300km of the Earth's inner core inferred from global array data: I. Regional 1D attenuation and velocity profiles. *Physics of the Earth and Planetary Interiors*, *230*, 15–27. https://doi.org/10.1016/j.pepi.2014.02.002

Iritani, R., Takeuchi, N., & Kawakatsu, H. (2014b). Intricate heterogeneous structures of the top 300 km of the Earth's inner core inferred from global array data: II. Frequency dependence of inner core attenuation and its implication. *Earth and Planetary Science Letters*, *405*, 231–243. https://doi.org/10.1016/j.epsl.2014.08.038

Irving, J. C. E., & Deuss, A. (2011). Hemispherical structure in inner core velocity anisotropy. *Journal of Geophysical Research*, *116*, B04307. https://doi.org/10.1029/2010JB007942

Irving, J. C. E., & Deuss, A. (2015). Regional seismic variations in the inner core under the North Pacific. *Geophysical Journal International*, *203*(3), 2189–2199. https://doi.org/10.1093/gji/ggv435

Ishii, M., Dziewonski A. M., Tromp J., & Ekström G. (2002). Joint inversion of normal mode and body wave data for inner core anisotropy 2. Possible complexities. *Journal of Geophysical Research*, *107*(B12), 2380. https://doi.org/10.1029/2001JB000713

Ishii, M., Tromp J., Dziewonski A. M., & Ekström G. (2002). Joint inversion of normal mode and body wave data for inner core anisotropy 1. Laterally homogeneous anisotropy. *Journal of Geophysical Research*, *107*(B12), 2379. https://doi.org/10.1029/2001JB000712

Kennett, B. L. N., Engdahl, E. R., & Buland, R. (1995). Constraints on seismic velocities in the Earth from traveltimes. *Geophysical Journal International*, *122*(1), 108–124. https://doi.org/10.1111/j.1365-246X.1995.tb03540.x

Lay, T., & Helmberger, D. V. (1983). A lower mantle *S*-wave triplication and the shear velocity structure of *D″*. *Geophysical Journal of the Royal Astronomical Society*, *75*(3), 799–837. https://doi.org/10.1111/j.1365-246X.1983.tb05010.x

Leykam, D., Tkalčić, H., & Reading, A. M. (2010). Core structure re-examined using new teleseismic data recorded in Antarctica: Evidence for, at most, weak cylindrical seismic anisotropy in the inner core. *Geophysical Journal International*, *180*(3), 1329–1343. https://doi.org/10.1111/j.1365-246X.2010.04488.x

Nissen-Meyer, T., van Driel, M., Stähler, S. C., Hosseini, K., Hempel, S., Auer, L., … Fournier, A. (2014). AxiSEM: Broadband 3-D seismic wavefields in axisymmetric media. *Solid Earth*, *5*(1), 425–445. https://doi.org/10.5194/se-5-425-2014

Romanowicz, B., Tkalčlč, H., & BréGer, L. (2003). On the origin of complexity in *PKP* travel time data. In *Earth's core: Dynamics, structure, rotation* (pp. 31–44). Washinton, DC: American Geophysical Union. https://doi.org/10.1029/GD031p0031

Romanowicz, B., & Wenk, H.-R. (2017). Anisotropy in the deep Earth. *Physics of the Earth and Planetary Interiors*, *269*, 58–90. https://doi.org/10.1016/j.pepi.2017.05.005

Shearer, P. M., Hedlin, M. A. H., & Earle, P. S. (1998). *PKP* and *PKKP* precursor observations: Implications for the small-scale structure of the deep mantle and core. In *The core-mantle boundary region* (pp. 37–55). Washington, DC: American Geophysical Union. https://doi.org/10.1029/GD028p0037

Shearer, P. M., & Toy, K. M. (1991). PKP (BC) versus PKP (DF) differential travel times and aspherical structure in the Earth's inner core. *Journal of Geophysical Research*, *96*, 2233–2247. https://doi.org/10.1029/90JB02370

Simmons, N. A., Myers, S. C., Johannesson, G., Matzel, E., & Grand, S. P. (2015). Evidence for long-lived subduction of an ancient tectonic plate beneath the southern Indian Ocean. *Geophysical Research Letters*, *42*, 9270–9278. https://doi.org/10.1002/2015GL066237

Song, X., & Helmberger, D. V. (1993). Anisotropy of Earth's inner core. *Geophysical Research Letters*, *20*, 2591–2594. https://doi.org/10.1029/93GL02812

Song, X., & Helmberger, D. V. (1998). Seismic evidence for an inner core transition zone. *Science*, *282*(5390), 924–927. https://doi.org/10.1126/science.282.5390.924

Song, X., & Xu, X. (2002). Inner Core transition zone and anomalous PKP(DF) waveforms from polar paths. *Geophysical Research Letters*, *294*, 1042. https://doi.org/10.1029/2001GL013822

Sun, D., Helmberger, D., Miller, M. S., & Jackson, J. M. (2016). Major disruption of D″ beneath Alaska. *Journal of Geophysical Research: Solid Earth*, *121*, 3534–3556. https://doi.org/10.1002/2015JB012534

Sun, X., & Song, X. (2008). Tomographic inversion for three-dimensional anisotropy of Earth's inner core. *Physics of the Earth and Planetary Interiors*, *167*(1-2), 53–70. https://doi.org/10.1016/j.pepi.2008.02.011

Sun, X., Song, X., Zheng, S., & Helmberger, D. V. (2007). Evidence for a chemical-thermal structure at base of mantle from sharp lateral P-wave variations beneath Central America. *Proceedings of the National Academy of Sciences of the United States of America*, *104*(1), 26–30. https://doi.org/10.1073/pnas.0609143103

Suzuki, Y., Kawai, K., Geller, R. J., Borgeaud, A. F. E., & Konishi, K. (2016). Waveform inversion for 3-D S-velocity structure of D′′ beneath the northern Pacific: Possible evidence for a remnant slab and a passive plume. *Earth, Planets and Space*, *68*(1), 198. https://doi.org/10.1186/s40623-016-0576-0

Tanaka, S., & Hamaguchi, H. (1997). Degree one heterogeneity and hemispherical variation of anisotropy in the inner core from PKP(BC)-PKP(DF) times. *Journal of Geophysical Research*, *102*, 2925–2938. https://doi.org/10.1029/96JB03187

Tkalčić, H. (2010). Large variations in travel times of mantle-sensitive seismic waves from the south Sandwich Islands: Is the Earth's inner core a conglomerate of anisotropic domains? *Geophysical Research Letters*, *37*, L14312. https://doi.org/10.1029/2010GL043841

Tkalčić, H., Romanowicz, B., & Houy, N. (2002). Constraints on D″ structure using PKP(AB-DF), PKP(BC-DF) and PcP-P traveltime data from broad-band records. *Geophysical Journal International*, *149*(3), 599–616. https://doi.org/10.1046/j.1365-246X.2002.01603.x

Wen, L., & Niu, F. (2002). Seismic velocity and attenuation structures in the top of the Earth's inner core. *Journal of Geophysical Research*, *107*(B11), 2273. https://doi.org/10.1029/2001JB000170

Wessel, P., & Smith, W. H. F. (1991). Free software helps map and display data. *Eos, Transactions American Geophysical Union*, *72*(41), 441–446. https://doi.org/10.1029/90EO00319

Yao, Y., Whittaker, S., & Thorne, M. S. (2015). D″ discontinuity structure beneath the North Atlantic from Scd observations. *Geophysical Research Letters*, *42*, 3793–3801. https://doi.org/10.1002/2015GL063989

Young, M. K., Tkalčić, H., Bodin, T., & Sambridge, M. (2013). Global P wave tomography of Earth's lowermost mantle from partition modeling. *Journal of Geophysical Research*, *118*, 5467–5486. https://doi.org/10.1002/jgrb.50391